



Obrabotka metallov -

Metal Working and Material Science







Journal homepage: http://journals.nstu.ru/obrabotka_metallov



Information properties of vibroacoustic emission in diagnostic systems for cutting tool wear

Vilor Zakovorotny ^a, Valery Gvindjiliya ^{b, *}, Kirill Kislov ^c

Don State Technical University, 1 Gagarin square, Rostov-on-Don, 344000, Russian Federation

^a  <https://orcid.org/0000-0003-2187-9897>,  vzakovorotny@dstu.edu.ru; ^b  <https://orcid.org/0000-0003-1066-4604>,  vgvindjiliya@donstu.ru;
^c  <https://orcid.org/0000-0002-5770-2519>,  kislovk@bk.ru

ARTICLE INFO

Article history:

Received: 19 April 2025

Revised: 23 April 2025

Accepted: 05 June 2025

Available online: 15 September 2025

Keywords:

Cutting tool condition diagnostics

Vibrations

Information models of dynamic monitoring

ABSTRACT

Introduction. This paper is devoted to the development of a methodology for diagnosing cutting tool wear based on the analysis of vibroacoustic emission signals. Two tasks are addressed. Firstly, the information feature space related to wear is constructed. Secondly, within this space, decision rules are defined that allow division into separate clusters according to wear levels. Since the construction of the information feature space (*IFS*) methods is of primary importance in these procedures, the **purpose of this work** is to determine the regularities of changes in the frequency characteristics of the dynamic cutting system caused by wear development and to construct, on this basis, a rational information space for diagnosing tool wear. **Method and methodology.** The study is based on mathematical modeling results of a perturbed dynamic cutting system to determine the information feature space representing tool wear. Methods for determining the parameters of information signal parameters (*ISPs*) are proposed, which provide high sensitivity to wear changes. All *ISP* parameters should be dimensionless and zeroed at zero wear. They must satisfy additional requirements, including noise immunity conditions. **Results and discussion.** The paper presents results of constructing *ISP* parameters for vibroacoustic emission analysis in two frequency ranges. In the low-frequency range, limited by the first natural frequencies of interacting subsystems (up to 1.0–1.5 kHz), vibration response parameters (*VRP*) are determined based on vibration sequences obtained analytically under power perturbations modeled as “white” noise. In the high-frequency range (above 2.0 kHz), information models based on random pulse sequences are proposed. It is shown that the applicability of a particular information feature depends on the conditions. Thus, the developed methodology, mathematical simulation, and digital and field experiments enabled the formation of a rational information space for wear diagnostics, in which known recognition methods can be used to construct decision rules for classifying information according to wear levels.

For citation: Zakovorotny V.L., Gvindjiliya V.E., Kislov K.V. Information properties of vibroacoustic emission in diagnostic systems for cutting tool wear. *Obrabotka metallov (tekhnologiya, oborudovanie, instrumenty)* = *Metal Working and Material Science*, 2025, vol. 27, no. 3, pp. 50–70. DOI: 10.17212/1994-6309-2025-27.3-50-70. (In Russian).

Introduction

In recent years (10–15), the global scientific community has been focusing on the construction of virtual digital models (*VDM*) of machining [1–14]. These models are primarily designed to determine the relationship between technological parameters and the output properties of the machining process. Most of the presented works do not reveal the structure of the relationship between state coordinates and output properties [1–7], but use experimentally obtained regression equations that couple technological parameters to the quality parameters of parts and tool wear [5–7]. This information is necessary for constructing a *CNC* program. In many cases, neural network modeling methods are used instead of regression equations [8–11]. The exceptions are studies [2–4, 17–21], in which dynamic cutting system (*DCS*) models are used to construct *VDM*. *VDMs* have been developed that allow the trajectories of form-forming movements to be

* Corresponding author

Gvindjiliya Valery E., Ph.D. (Engineering), Senior Lecturer
Don State Technical University,
1 Gagarin square,
344000, Rostov-on-Don, Russian Federation
Tel.: +7 918 583-23-33, e-mail: vgvindjiliya@donstu.ru

coupled to the geometric characteristics of the formed surface and wear [17–21]. Most studies are limited to the problem of estimating wear as the main factor affecting the output properties [22–24]. Here, we note the modeling of evolutionary changes in the *DCS* that we proposed earlier [25, 26]. In this system, wear evolution and quality parameters are represented as a *Volterra's* integral equation of the second kind with respect to the phase trajectory of irreversible transformations in terms of work done. Thus, the evolution of properties and parameters reveals the complete *DCS*. However, its use requires significant computing resources. In this paper, we will limit ourselves to the problem of wear diagnosis based on the analysis of vibroacoustic emission (*VAE*) [27–47]. To measure *VAE*, piezoelectric transducers, force sensors, non-contact laser and other measuring systems are used to determine the vibrations of a certain *DCS* coordinate in the frequency range (10 Hz...600 kHz). The measured sequences undergo preliminary processing using integral transformations, primarily *Fourier* transformations [26], *Wavelet* transformations [37], *Hilbert-Huang* transformations [36], *Volterra* transformations [3, 37, 28], etc. Methods of complexing measurable sequences of various physical nature are used [48].

In contrast to previous studies, this paper focuses on the construction of an information sign space (*ISS*), which considers the sensitivity of parameters' variations to wear changes, their noise immunity, and ease of formation in diagnostic systems. Two frequency ranges are considered separately. The low-frequency range is within (1.0–1.5) kHz, and the high-frequency range is above 2.0 kHz. This division is due to the peculiarities of mathematical modeling of the *DCS* as a channel through which information about the force interactions formed during processing is transmitted.

The purpose of the work is to develop a method for diagnosing cutting tool wear by determining the information space of features formed on the basis of studying changes in the frequency characteristics of the dynamic cutting system caused by wear development. To achieve this purpose, the following tasks must be undertaken.

- to develop an analytical method for determining the information space of the low- and high-frequency ranges;
- to perform mathematical modeling and to conduct digital simulations, and full-scale experiments;
- to determine the parameters of the information space within the considered frequency ranges and a method for their evaluation.

Methods

Methodology for experimental wear assessment

A generalized parameter for assessing the tool's condition is the wear on its flank face. Therefore, let us consider an algorithm for the experimental assessment of flank wear, which is defined by the height of the flank wear land (Fig. 1). The configuration of the wear mark on the flank face varies, and only in some cases does it approximate a rectangle, as shown in Fig. 1, *a*. Therefore, we will define the wear assessment as the height of an equivalent rectangle, $w = S_0 / (t_p^{(0)} - X_l^*)$, where S_0 is the surface area of the wear trace on the flank face of the tool, and X_l^* is the elastic deformation under equilibrium conditions. The area S_0 is estimated using a grid (Fig. 1, *c*). It has been previously shown [2, 3, 26, 47] that the properties of dynamic contact stiffness (*DCS*) are influenced by dynamic connection parameters, and changes in these parameters are manifested as variations in vibration spectra. The parameters of this connection are dependent on wear, and it is convenient to analyze the interdependence of the vibration spectrum and wear independently within two frequency ranges. In the low-frequency range ($\omega_H \in (0, \omega_0)$), the model can be represented as a finite-dimensional spatial discrete model [47]. This is a frequency range whose upper limit is defined by the natural frequencies of the tool and workpiece subsystems. We will interpret the frequency range above ω_0 as the high-frequency range ($\omega_B \in (\omega_0, \infty)$).

Methodology for analytical determination of the information space in the low-frequency range

The previously derived *DCS* model [47] is considered. We will limit our analysis to the case of machining a non-deformable workpiece. Then, the equation of the perturbed dynamic system response (*DSR*) can be written as:

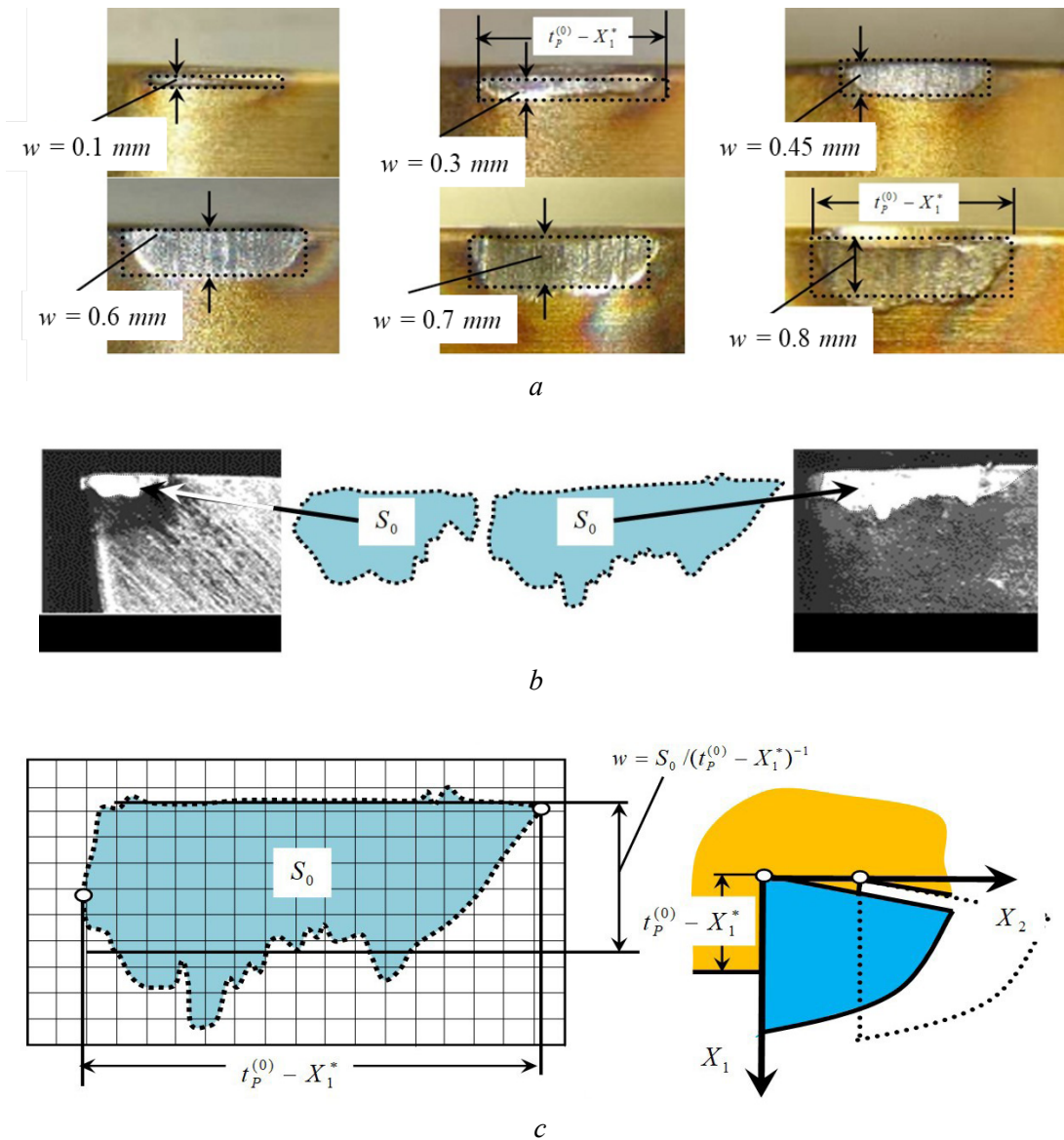


Fig. 1. Examples of photographs of the worn tool part and wear evaluation scheme:

a – flank wear of a 79 WC-15 TiC-6% Co insert during turning of AISI 301 steel; *b* – wear development of a 79 WC-15 TiC-6% Co insert during turning of steel 0.2 C-Cr; *c* – schematic of the matrix grid

$$\mathbf{m} \frac{d^2 \mathbf{X}}{dt^2} + \mathbf{h} \frac{d \mathbf{X}}{dt} + \mathbf{c} \mathbf{X} = \mathbf{F}_{\Sigma}(\mathbf{L}, \mathbf{V}, \mathbf{X}, \mathbf{p}) + \mathbf{f}(t) \quad (1)$$

where $\mathbf{m} = \text{diag}(m)$, $\mathbf{h} = [h_{s,k}]$, $\mathbf{c} = [c_{s,k}]$, \mathbf{S} , $k = 1, 2, 3$ is positively definite symmetric matrices of inertial, velocity, and elastic coefficients; $\mathbf{X} = \{X_1, X_2, X_3\}^T \in \mathcal{R}_X^{(3)}$ is deformation vector; $\mathbf{F}_{\Sigma} = \mathbf{F} + \mathbf{\Phi}$ is the vector-function of forces on the rake \mathbf{F} and flank $\mathbf{\Phi}$ faces; $\mathbf{F} = \{F_1, F_2, F_3\}^T \in \mathcal{R}_X^{(3)}$; $\mathbf{\Phi} = \{\Phi_1, \Phi_2, \Phi_3\}^T \in \mathcal{R}_X^{(3)}$.

Let us also consider deformation velocities $\mathbf{V}_X = d\mathbf{X} / dt = \{V_{X,1}, V_{X,2}, V_{X,3}\}^T \in \mathcal{R}_X^{(3)}$. We represent forces \mathbf{F} in the form $\mathbf{F} = \{F_1, F_2, F_3\}^T = F^{(0)} \{\chi_1, \chi_2, \chi_3\}^T$ [47]. Here χ_1, χ_2, χ_3 are angular coefficients satisfying the condition $(\chi_1)^2 + (\chi_2)^2 + (\chi_3)^2 = 1$. The given perturbations $\mathbf{f}(t) = f_0(t) \{\chi_1, \chi_2, \chi_3\}^T$ are considered to be reduced to the coordinate system of the forces \mathbf{F} . Furthermore, $f_0(t)$ is modeled as “white” noise. Based on prior studies, the model of cutting forces acting on the rake face of the tool $F^{(0)}$ is given by [47]:

$$T^{(0)} dF^{(0)} / dt + F^{(0)} = \rho(V_3, V_{X_3}) \left\{ t_p^{(0)} - [X_1 - k_p X_1(t - T)] \right\} \times \int_{t-T}^t \{V_2(\xi) - V_{X_2}(\xi)\} d\xi, \quad (2)$$

where $\rho = \rho_0 \{1 + \mu \exp[-\zeta(V_3 - V_{X_3})]\}$ is the chip pressure, kg/mm²; ρ_0 is the pressure in the area of low cutting speed region on the tool's rake face; μ is the dimensionless parameter; ζ is the steepness coefficient, s/m; $T^{(0)}$ is the chip formation time constant, s; k_p is the dimensionless trail regeneration coefficient ($0 < k_p \ll 1$).

Forces Φ_2, Φ_3 can be expressed as:

$$\begin{aligned} \Phi_2 &= k_\Phi F_0 + \rho_\Phi [t_p^{(0)} - X_1(t)] \exp[\zeta(v - v^*)]; \\ \Phi_3 &= k_\Phi k_T F_0 + k_T \rho_\Phi \left\{ (t_p^{(0)} - X_1(t)) \exp[\zeta(v - v^*)] \right\}, \end{aligned} \quad (3)$$

where ρ_Φ is the force per unit contact length on the tool flank face, representing stiffness, kg/mm; ζ is a parameter depending on the rear angle α and wear; k_T is the friction coefficient; k_Φ is the dimensionless coefficient of elastic recovery.

Equations (1)-(3) constitute a numerical model of the DCS. The model's adequacy was validated by comparing the results of digital simulations and full-scale experiments, which were conducted using continuous vibration monitoring measurement systems. The parameters of the dynamic connection equation, particularly the chip pressure on the rake face of the tool, were refined using both theoretical material [49] and force measurements during the cutting process [50]. For this purpose, a STD.201-1 system was used instead of the support to measure the dynamic loads on the tool along the $\{X_1, X_2, X_3\}$ axes. The hardware interface of the test bench consists of a set of electronic units manufactured by National Instruments: NI-9234, NI-9237, and NI-9219, with a sampling frequency of up to 25 kHz. The accuracy of the analytical simulation results is limited by the zone of steady-state tool wear and the onset of accelerated wear, where the influence of random processes in the cutting zone reduces the accuracy of classical analytical nonlinear models.

Here, we leverage previously developed mathematical tools to construct a space of wear characteristics.

It is important to note that the parameters of the dynamic connection $\mathbf{p}(\mathbf{w}) = \{p_1(\mathbf{w}), p_2(\mathbf{w}), \dots, p_n(\mathbf{w})\}$ formed during cutting depend on wear. Let experimentally determined trajectories be given as $\mathbf{p}(\mathbf{w}) = \{p_1(\mathbf{w}), p_2(\mathbf{w}), \dots, p_n(\mathbf{w})\}$. For the sequence $\mathbf{w} = \{w_1, w_2, \dots, w_k\}$, we calculate the spectra $S_{X_1, X_1}(\omega)$, $S_{X_2, X_2}(\omega)$ and $S_{X_3, X_3}(\omega)$ in the space $\mathfrak{R}_X^{(3)}$ as Fourier transforms of the diagonal elements of the correlation matrices of the time series of deformations $X^{(i)}(t) = \{X_1^{(i)}(t), X_2^{(i)}(t), X_3^{(i)}(t)\}^T \in \mathfrak{R}_X^{(3)}$, $i = 1, 2, \dots, k$. Consequently, we obtain a set of deformation spectra for each set of parameters corresponding to each wear state $\mathbf{w} = \{w_1, w_2, \dots, w_k\}$.

Results and Discussion

Example of determining the parameters of the information space in the low-frequency range

If the perturbations $f_0(t)$ are small and the equilibrium is asymptotically stable, then the forces Φ in Equation (1) can be neglected. In this case, the main parameters influencing the formation of the spectra are the variations in ρ and $T^{(0)}$. Consider the turning of a shaft with a diameter of $D = 84.0$ mm, made of 0.1 C-Mn-2 Ni-Mo-V steel. The investigations were carried out as part of the implementation of a commercial contract with Atomash (Volgodonsk). The machining conditions were based on the technological process for manufacturing a real "blow-off pipe" type detail for rough turning. The technological parameters were as follows: feed rate $S_p = 0.1$ mm; depth of cut $t_p = 2$ mm; and cutting speed $V_3 = (0.5 \dots 3.8)$ m/s. During the investigation, the range of cutting speeds was expanded in order to obtain more complete information

about the diagnostic characteristics in the vibroacoustic emission (*VAE*) signals. Machining was performed on a modernized *IK62* lathe, equipped with adjustable spindle and feed drives. Instead of the carriage, a *STD.201-1* measuring system was installed to determine forces, vibration, and temperature. Parameters are given in Table 1. The total mass is $m = 0.015 \text{ kg}\cdot\text{s}^2/\text{mm}$. The dynamic couple parameters are provided in Table 2. The resonant frequencies of the tool subsystem are $\Omega_{0,1} = 130 \text{ Hz}$, $\Omega_{0,1} = 174 \text{ Hz}$, $\Omega_{0,1} = 236 \text{ Hz}$.

Table 1

Matrices of speed coefficients and elasticity of the tool subsystem

$c_{1,1} \text{ (kg/mm)}$	$c_{2,2} \text{ (kg/mm)}$	$c_{3,3} \text{ (kg/mm)}$	$h_{1,1} \text{ (kg}\cdot\text{s/mm)}$	$h_{2,2} \text{ (kg}\cdot\text{s/mm)}$	$h_{3,3} \text{ (kg}\cdot\text{s/mm)}$
4,500	1,500	750	1.3	1.1	0.8
$c_{1,2} = c_{2,1}$ (kg/mm)	$c_{1,3} = c_{3,1}$ (kg/mm)	$c_{2,3} = c_{3,2}$ (kg/mm)	$h_{1,2} = h_{2,1}$ (kg·s/mm)	$h_{1,3} = h_{3,1}$ (kg·s/mm)	$h_{2,3} = h_{3,2}$ (kg·s/mm)
200	150	80	0.6	0.5	0.4

Table 2

Dynamic coupling parameters

ρ (kg/mm ²)	ρ_ϕ (kg/mm ²)	$\Omega \text{ (s}^{-1}\text{)}$	$T^{(0)} \text{ (s)}$	ζ	k_T	$k^{(T)}$ (s/m)	$k^{(S)}$	χ_1	χ_2	χ_3
100–1,000	20	5–50	0.0001	1–7	0.2	5	0.1	0.4	0.51	0.76

The spectra are studied based on numerical modeling in the *Matlab-Simulink* software package, as well as experimentally by direct measurement of the vibroacoustic emission (*VAE*) during the cutting process. Let us consider the spectra of deformation oscillations $X \in \mathfrak{R}_X^{(3)}$ calculated as responses to “white” noise. The spectra in Fig. 2, *a* and *b* differ from the spectrum in Fig. 2, *c* by angular coefficients $\chi = \{\chi_1, \chi_2, \chi_3\}^T$. The examples are selected to illustrate the following properties of the spectra.

1. Resonances (shown as round, unshaded points) and antiresonances (shown as shaded points) can be distinguished in the spectrum. In real systems, they remain virtually unchanged when the parameters of the dynamic connection formed by the cutting process vary.

2. In the case of kinematic disturbances (Fig. 2, *a*), periodic spikes are superimposed on the spectra. The distance between them is equal to the rotation frequency of the workpiece. In the case of force disturbances, the peaks are normalized (Fig. 2, *b*). They are also normalized in the high-frequency range. Therefore, in the actual measured spectrum, significant variations in level are detected as the frequency increases, but resonance frequencies are usually observed.

3. Peaks at all resonances may not appear, or they may appear to a lesser extent (Fig. 2, *c*). This behavior is determined by the structure of the elasticity matrices c coefficients χ . It is known that the angular coefficients change as wear increases. For example, forces in the direction normal to the flank face increase faster [51], which is reflected in the redistribution of amplitudes at resonance frequencies.

4. Wear development causes an increase in the parameters ρ and $T^{(0)}$, as well as a change in the angular coefficients χ . An increase in ρ causes a shift in the roots of the characteristic polynomial of the linearized variation equation, such that some roots move toward the imaginary axis, and an increase in ρ always leads to a loss of stability. An increase in $T^{(0)}$ has a contradictory effect. On the one hand, an increase in $T^{(0)}$ contributes to self-excitation, and on the other hand, it leads to additional damping.

5. As wear progresses, due to changes in the parameters of dynamic coupling, the system may lose its equilibrium stability, and various attracting sets of deformations may form in the vicinity of the trajectory,

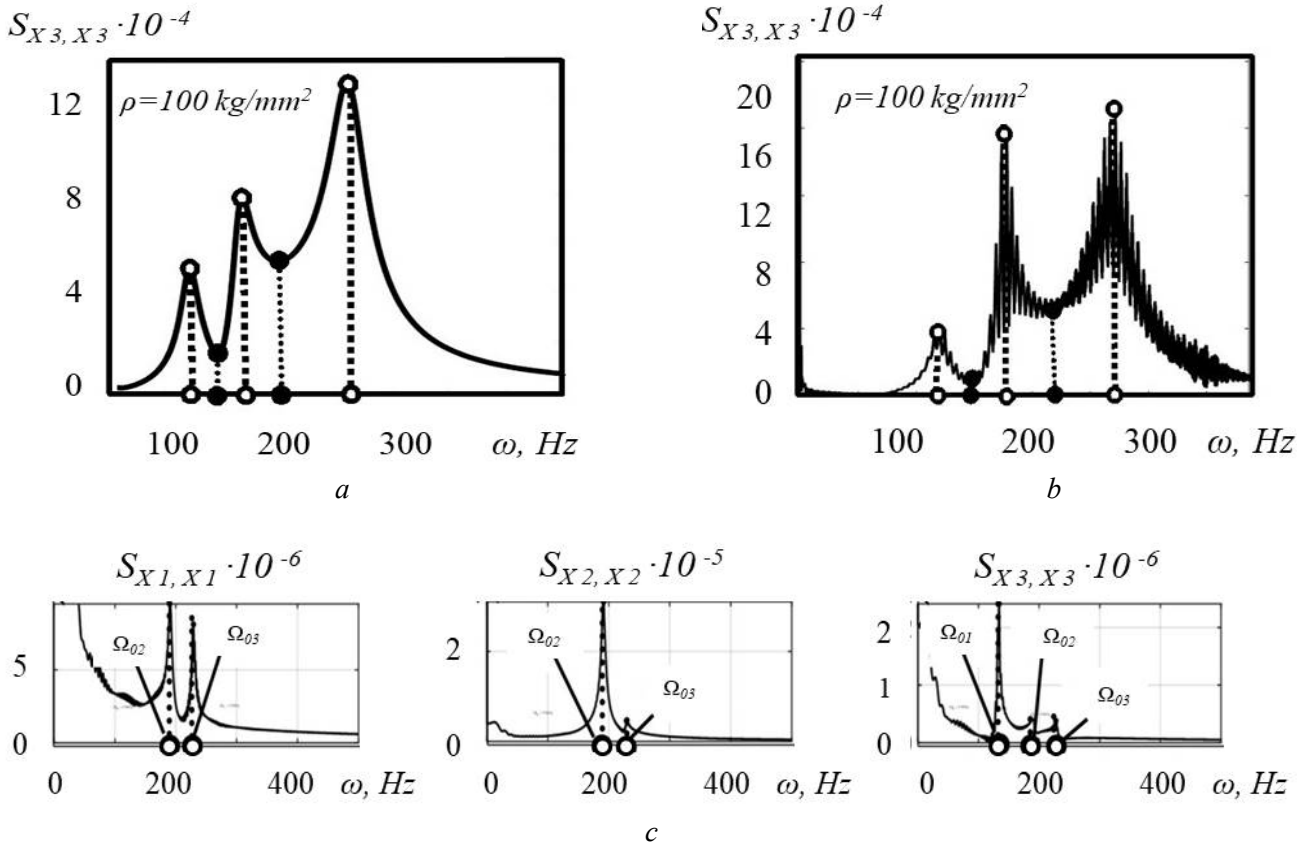


Fig. 2. Typical examples of autospectra:

a – spindle rotation frequency of 10.0 Hz, disturbances applied to feed rate variations; *b* – spindle rotation frequency of 100 Hz, disturbances applied to cutting force module; *c* – spectral changes depending on the direction of deformation displacements in space $\mathfrak{R}_X^{(3)}$

with bifurcations possibly observed along the trajectory. In this case, the normalized vibration spectrum is practically independent of perturbations and is determined by the properties of the DCS.

An example of the influence of parameter ρ on the dispersion-normalized spectrum for value $X \in \mathfrak{R}_X^{(3)}$ is shown in Fig. 3. Experiments show that for 0.1 C-Mn-2 Ni-Mo-V steel under conditions of feed rate $S_p^{(0)} = 0.1 \text{ mm}$, cutting depth $t_p^{(0)} = 1.5 \text{ mm}$, and cutting speed $V_3^{(0)} = 1.2 \text{ m/s}$, as wear on the rake face increases to 0.6 mm, a monotonic increase in ρ from 100 kg/mm^2 to 160 kg/mm^2 is observed. This corresponds to the transformation of the spectrum shown in Fig. 4.

Note the special features of the spectrum changes. There is a redistribution of the intensity of oscillations in frequency ranges located near the natural frequencies. Let us denote them by $A_{i,s}$, $i, s = 1, 2, 3$. Here, i is the resonance number, and s is the number of directions of oscillations in space $\mathfrak{R}_X^{(3)}$. As ρ increases, not only does the amplitude at frequency Ω_3 increase, but the quality factor of this mode also increases. At $\rho = 160 \text{ kg/mm}^2$ a single oscillator with a common frequency Ω_3 is formed. Analysis shows that when $\rho = 145 \text{ kg/mm}^2$, the equilibrium loses stability and self-oscillations are formed.

More details on the formation of attracting sets of deformations can be found in our works [2, 3, 25, 26]. As the roots of the characteristic polynomial approach the imaginary axis, the quality factor of the oscillator representing this pair of complex conjugate roots increases. Here are some examples of how the ratio of amplitudes at resonances changes with ρ (Fig. 4). The point of instability is marked with a red dotted line, to the right of which a delta-shaped spectrum $\delta(\omega - \Omega_3)$ is formed, so all coefficients increase indefinitely.

A rougher but more interference-resistant estimate is the average frequency of the spectrum $\omega^{(C)}$ in the $X \in \mathfrak{R}_X^{(3)}$ directions. With increasing wear, primarily due to an increase in the parameter $T^{(0)}$, a shift of the

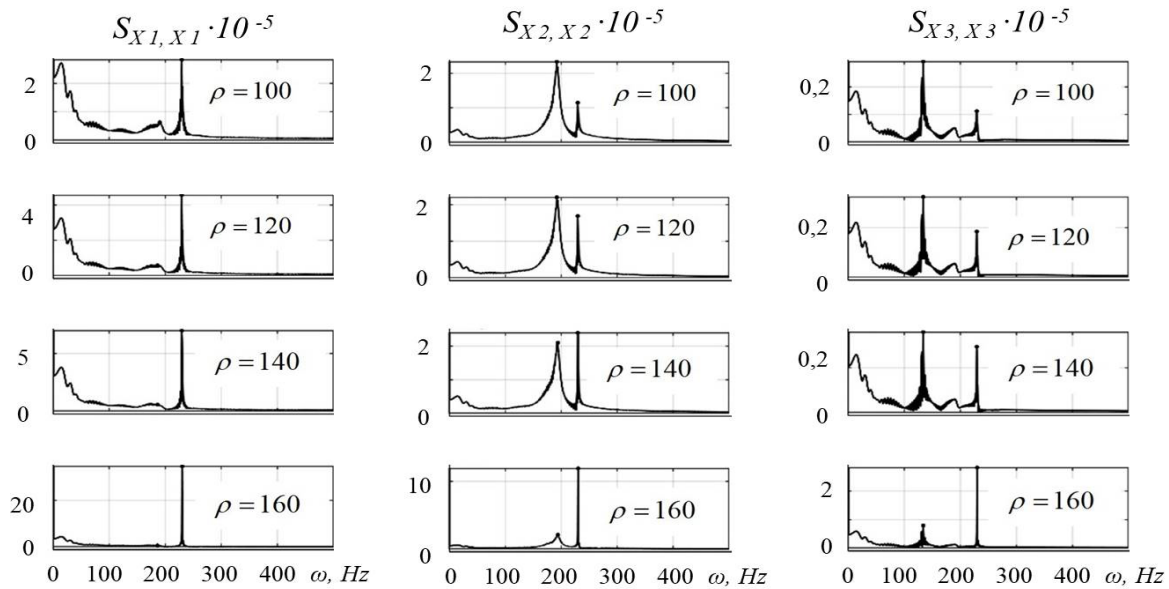


Fig. 3. Example of changes in deformation autospectra depending on chip pressure ρ on the tool's rake face

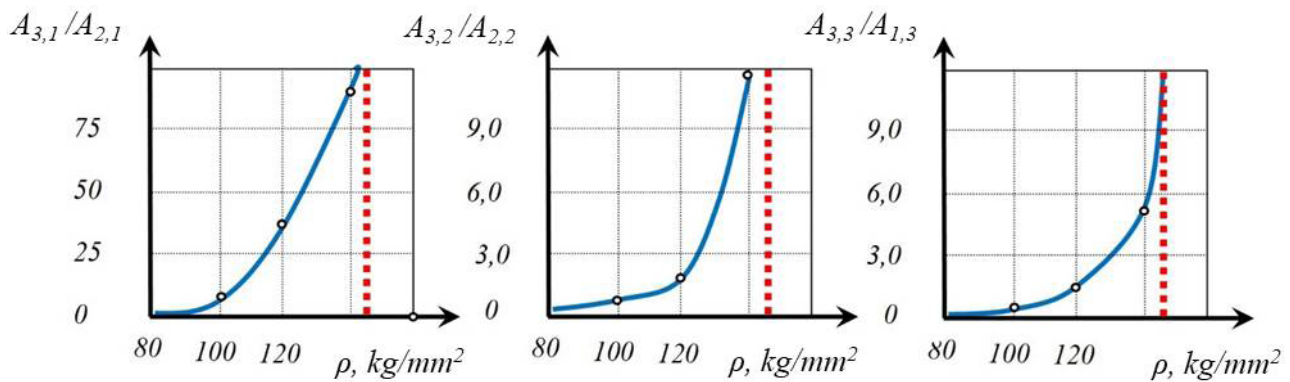


Fig. 4. Sensitivity of amplitudes at resonances to variations ρ

overall vibration spectrum toward the low-frequency range is observed. If $\omega^{(C)}$ is specified, then $\int_0^{\omega^{(C)}} S_{X_i X_i}(\omega) d\omega = \int_{\omega^{(C)}}^{\infty} S_{X_i X_i}(\omega) d\omega$ is valid. The increment $\omega^{(C)}$ depends less significantly on variations in

the initial parameters, disturbances, and modes.

As wear increases, two interrelated processes can be observed. The first process characterizes the determination of the state (Fig. 5). In this case, the peaks in the spectra become more pronounced and exhibit increased quality factors. The second process characterizes the degradation of properties, manifested in the formation of chaos.

Dispersion estimation is used to evaluate evolution

$$\hat{\sigma}_{X_1, X_1}(\rho_i) = \sigma_{X_1, X_1}(\rho_i) [\sigma_{X_1, X_1}(\rho_0)]^{-1}, \quad (4)$$

where $\sigma_{X_1, X_1}(\rho_i) = \frac{1}{\pi} \int_0^{\infty} S_{X_1, X_1}(\omega, \rho_i) d\omega$, $i = 0, 1, 2 \dots k$; $\mathbf{\rho} = \{\rho_0, \rho_1, \dots, \rho_r\}$ is sequence of ρ_i values, each of

which corresponds to a variance.

In this regard, when considering the total variance, there are two stages (Fig. 5, b).

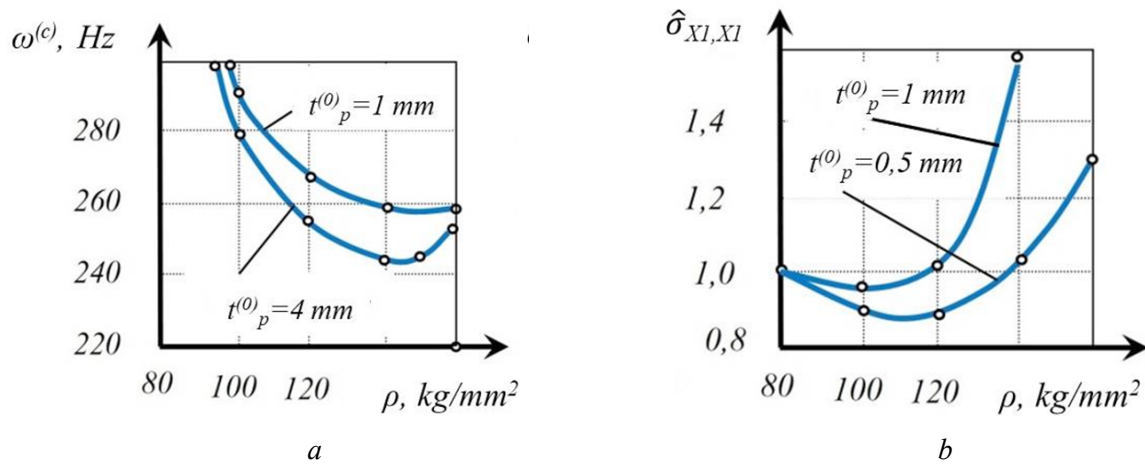


Fig. 5. Sensitivity of average frequency $\omega^{(c)}$ (a) and relative dispersion $\sigma_{X1,X2}$ (b) during variation at different cutting depths $t_p^{(0)}$

At the initial stage of running-in, the dispersion of oscillations decreases, and then increases. This trend holds true regardless of whether the equilibrium point is stable or whether various attracting sets of deformations form in its vicinity. The analysis allows us to create an *ISS* system. The first assessment Π_1 is based on an analysis of changes in relative amplitude $A_{i,s}$, $i, s = 1, 2, 3$ increments in the direction s :

$$\Pi_1 = [\delta_A(w) - \delta_A(0)] \delta_A(0)^{-1}, \quad (5)$$

where $\delta_A(w) = A_{3,1}(w) / A_{2,1}(w)$, $s = 1$.

The second Π_2 assessment is based on determining the $\omega^{(c)}$ displacement as w wear increases. However, calculating the average frequency requires significant computing resources. Therefore, an equivalent assessment of two signals passing through low- and high-frequency filters can be considered. In this case, it is not necessary for the cutoff frequencies of the filters to coincide exactly with the frequency $\omega^{(c)}$. Then,

$$\Pi_2 = \frac{\sigma_H(w) - \sigma_B(w)}{\sigma(w)}, \quad (6)$$

where $\sigma_H(w)$ is the dispersion of the *VAE* signal in the low-frequency range; $\sigma_B(w)$ is the dispersion of the *VAE* signal in the high-frequency range; $\sigma(w)$ is the general dispersion.

The signal processing is such that when $w = 0$, the assessment $\Pi_2 = 0$. Then, the assessment of Π_3 based on (4) is also informative:

$$\Pi_3 = \frac{\hat{\sigma}_{X1,X1}(w) - \hat{\sigma}_{X1,X1}(0)}{\hat{\sigma}_{X1,X1}(0)}, \quad (7)$$

where $\hat{\sigma}_{X1,X1}(w)$ is the dispersion assessment calculated using the algorithm in Eq. (4).

Parameters of the high-frequency range information space. In the high-frequency range, it is not possible to analytically determine the response of vibration sequences to changes in wear, since the dynamic model has a limited frequency range of validity. However, the cutting process is a source of waves in the frequency range reaching hundreds of kilohertz [5, 15]. We interpret the measured signal in the high-frequency range as an acoustic emission (*AE*) signal. The source of this signal is the force interactions in the regions (Fig. 6, *a*) of primary (1) and secondary (2) plastic deformation, as well as in the contact area between the flank face of the tool and the workpiece (3). When measuring this signal, the wave properties of the channel connecting the cutting zone with the *AE* measurement point are of fundamental importance. It is necessary to take into account not only the dissipative properties of the channel, but also its geometry, as well as joints that introduce nonlinear distortions and an insensitivity zone caused by butt joints [50, 51].

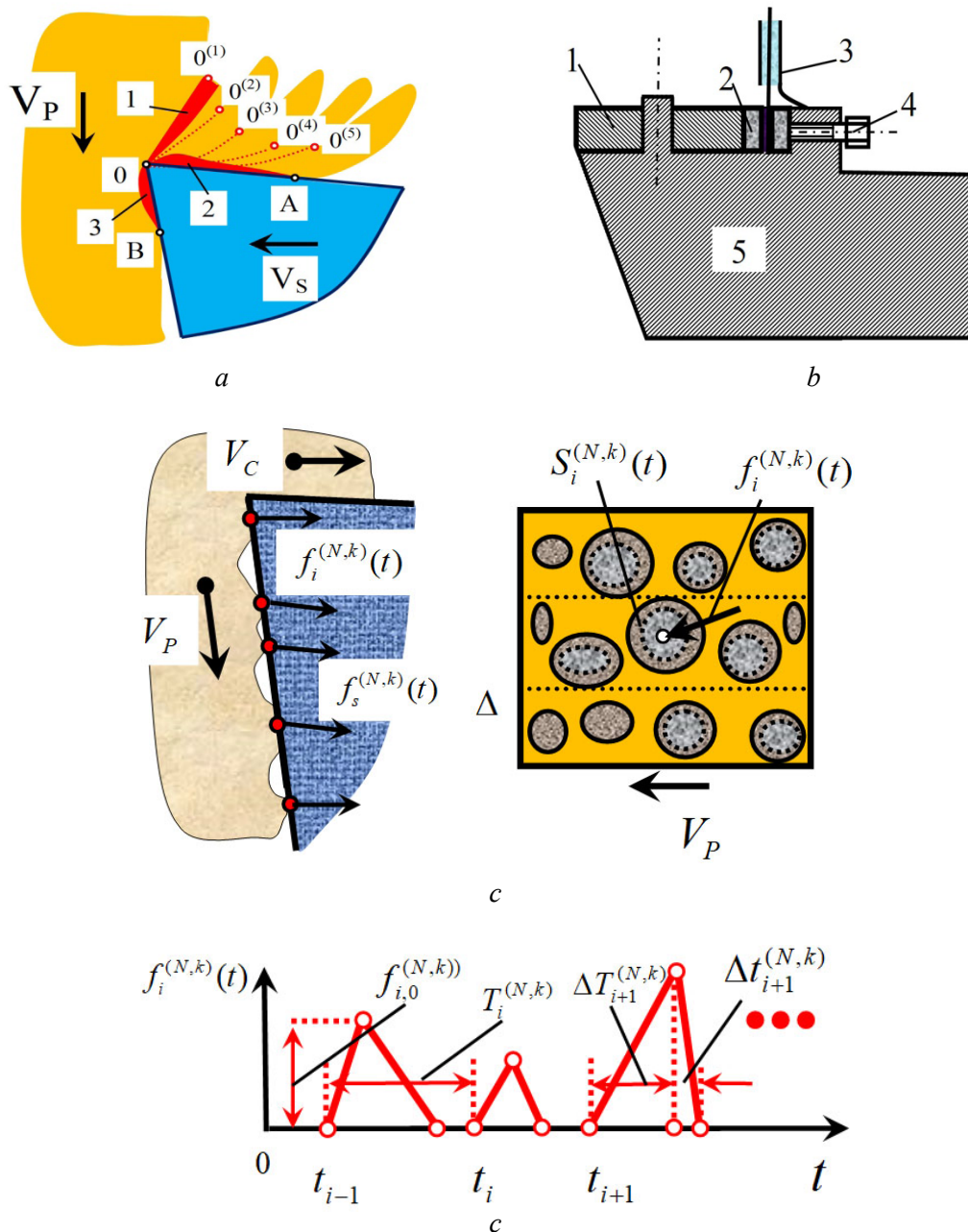


Fig. 6. Scheme of AE signal measurement and formation:

a – model of periodic force components formation; *b* – cutter measuring scheme; *c*, *d* – model of random pulse sequence formation

A measuring cutter (Fig. 6, *b*) was used for the experimental study of *AE* properties. *AE* was evaluated using a piezoelectric transducer (2) installed in contact with a tetrahedral plate (1) made of hardmetal (79 % *WC*; 15 % *TiC*) and the body of the cutter (5). Two ceramic plates, based on solid solutions of zirconate and lead titanate (*ZLT*), are installed so that their outer surfaces are in electrical contact with the tool body, while the central plates are insulated and connected to a coaxial cable (3), the braid of which is connected to the cutter body. The ceramic inserts (2) are pressed against the cutting plate with a screw (4). The coaxial cable is connected to a computer for information processing via an analog-to-digital converter *E14-440*.

A model of the source of power emission can be proposed. To do this, on the surface of the wearable flank face of the tool, we select the area of $S_i^{(N,k)}(t)$ (Fig. 6, *c*) in which the force $f_i^{(N,k)}(t)$ is formed. In time, it represents a sequence of standard pulses (Fig. 6, *d*), each of which describes the change in forces over a time interval $t \in (t_{i-1}, t_i)$.

$$f_i^{(N,k)}(t) = \begin{cases} f_i^{(N,k)}(t) = k_1^f t, & t \in (t_i, t_i + \Delta T_{i+1}^{(N,k)}), \quad k_1^f = f_{0,i}^{(N,k)} / \Delta T_{i+1}^{(N,k)}; \\ f_{0,i}^{(N,k)} - k_2^f t, & t \in (t_i + \Delta T_{i+1}^{(N,k)}, t_i + \Delta T_{i+1}^{(N,k)} + \Delta t_{i+1}^{(N,k)}), \quad k_1^f = f_{0,i}^{(N,k)} / \Delta t_{i+1}^{(N,k)}; \\ f_i^{(N,k)}(t) = 0, & t \in (t_i + \Delta T_{i+1}^{(N,k)} + \Delta t_{i+1}^{(N,k)}, t_{i+1}). \end{cases} \quad (8)$$

The sequence represents a set of standard pulses (8) $f_i^{(N,k)}(t) = \{f_i^{(N,k)}(t), t \in (0, T_1^{(N,k)}); f_i^{(N,k)}(t), t \in (T_1^{(N,k)}, T_2^{(N,k)}); \dots; f_i^{(N,k)}(t), t \in (T_{s-1}^{(N,k)}, T_s^{(N,k)})\}$. The tangential components of elementary forces $f_i^{(T,k)}(t)$ have a similar structure.

In the following, the work is limited to considering the impulse sequence $f_i^{(N,k)}(t)$, which has two stages. In the *first stage*, there is an accumulation of potential energy (time interval $\Delta T_{i+1}^{(N,k)}$). Here, elastic displacement of microcontacts occurs up to values at which the bonds break. This time depends on the cutting speed. In the *second stage*, the energy is released (time interval $\Delta t_{i+1}^{(N,k)}$). The release of energy is accompanied by an impulse of irreversible energy transformations, which generates heat, but also causes other physical interaction effects. The release of energy also forms an elastic wave impulse.

The standard sequence is characterized by the following parameters: the distance between pulses $T_i^{(N,k)}$, rise time $\Delta T_i^{(N,k)}$, fall time $\Delta t_i^{(N,k)}$, and height $f_{i,0}^{(N,k)}$ (Fig. 6, d). This impulse can be caused by elastic-plastic interaction or the destruction of adhesive and other bonds.

First, the frequency-domain representations of the sequence are analyzed (Fig. 7). In the illustration, the upper two curves represent the sequence in the time domain, but on different scales. The lower two diagrams correspond to their spectral representations, also shown on two scales. Note the following key properties of these representations.

1. If the distance between pulses is constant $T_i^{(N,k)} = 0.02 \text{ s} = \text{const}$, then the spectrum consists of a discrete set of frequencies depending on the pulse duration relative to the distance $\Delta T_i^{(N,k)}$. If the pulse width equals the distance between pulses, then in the frequency domain we observe frequency bursts corresponding to a *Fourier* series expansion. In this case, the spectrum contains constant components: the first and third harmonics (Fig. 7, a). When $\Delta T_i^{(N,k)}$ is reduced, additional frequencies appear (Fig. 7, b), which eventually transform into a continuous spectrum (Fig. 7, c). As $\Delta T_i^{(N,k)} \rightarrow 0$, the spectrum approaches “white” noise.

2. If uncertainty is introduced in $\Delta T_i^{(N,k)}$, then the discrete spectrum shown in Fig. 7, b transforms into a continuous spectrum (Fig. 7, d). A broadening of the spectral lines is observed. The frequency of the spectral maximum corresponds to the mathematical expectation of the distance between pulses, and the variability (spread) of the intervals between pulses is reflected in the broadening of the spectral line.

3. Changes in the ratio between the rising and falling stages of the pulses also affect the spectrum, but modeling shows that these changes are insignificant. Regarding amplitude uncertainty, the spectrum amplifies the components located between the main bursts. If a narrowband filter selects a signal in the frequency window $\Delta\omega$, an increase in amplitude uncertainty corresponds to an increase in amplitude modulation of the signal within this frequency window $\Delta\omega$.

In the contact region between the flank face of the tool and the workpiece, numerous interactions occur (Fig. 6, c), which generate the emission signal:

$$F^{(N)}(t) = \sum_{i=1}^{i=n} \sum_{k=1}^{k=m} f_i^{(N,k)}(t), \quad (9)$$

where k and i are the numbers of rows and contacts per row on the interaction surface, respectively.

It is necessary to formulate additional hypotheses regarding the influence of the probability distribution of these contacts on the contact surface in order to determine the spectral properties of the set of random sequences.

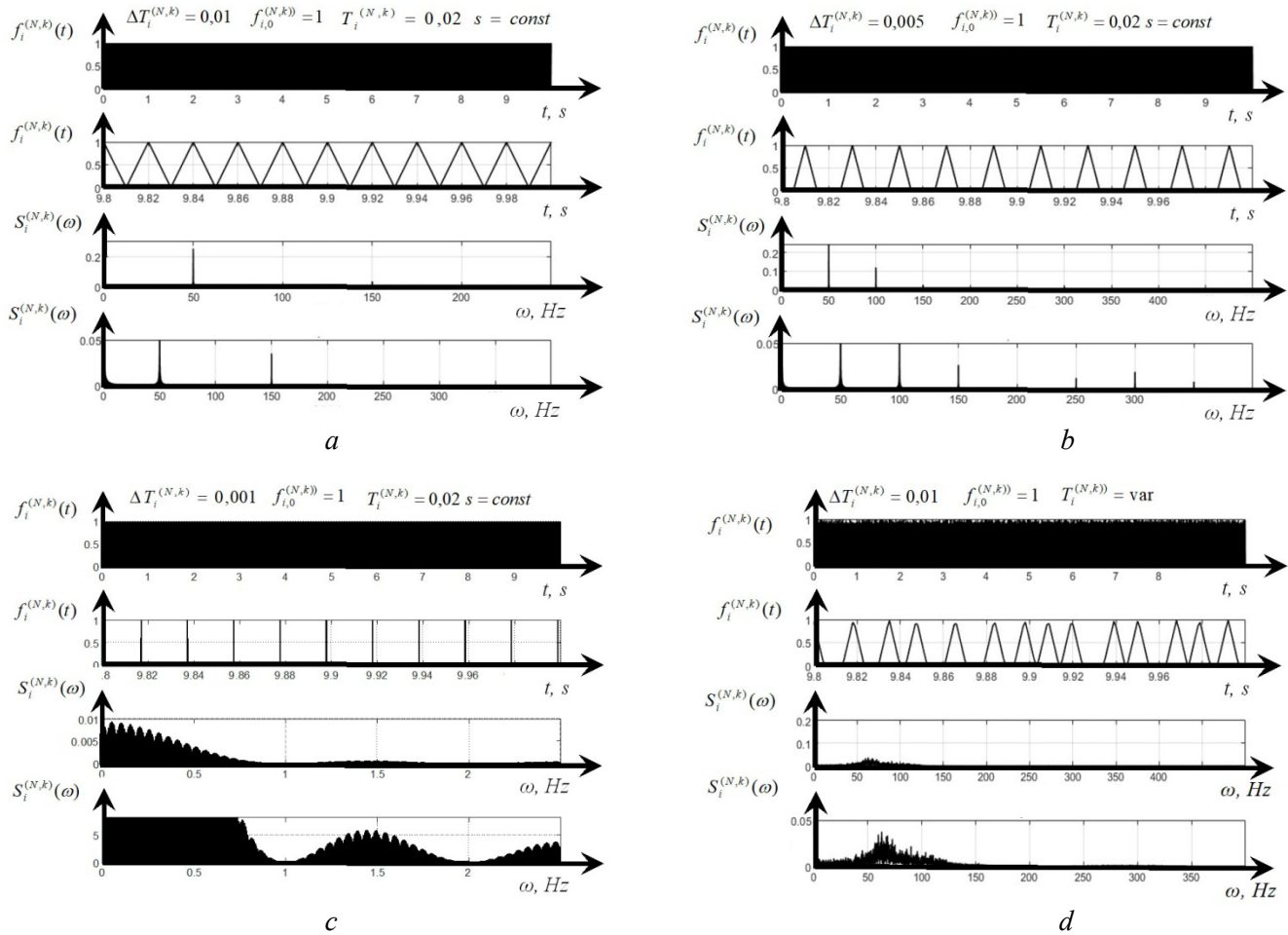


Fig. 7. Examples of spectral changes of a standard pulse sequence

The calculations indicate that increasing the uncertainty in the emission signal over time leads not only to broadening of the emission signal's spectral line but also to a decrease in the intervals between pulses due to regular spatial shifts in the signals. Therefore, as wear increases, the emission signal spectrum becomes blurred and shifts toward the high-frequency region. It is important to note that each individual pulse has risen and fall stages that depend primarily not on time but on the path of relative movements; thus, increasing the cutting speed reduces the parameters $T_i^{(N,k)}$ and $\Delta T_i^{(N,k)}$. As a result, the spectrum becomes dependent on the cutting speed.

If we analyze the frequency range $\Delta\omega_0 \in (\omega_{0,1}, \omega_{0,2})$, we observe that the main changes in the frequency spectra with increasing wear correspond to the features described above. Moreover, the upper frequency $\omega_{0,2}$ in this range is determined by the rule:

$$\omega_{0,2} = \left(\frac{h_0}{V_P} \right)^{-1}$$

where h_0 is the height of the contact between the flank face and the workpiece at the initial stage of wear $w = 0$; it depends on the elastic recovery of the material.

$$\text{The lower frequency is } \omega_{0,1} = \left(\frac{h_0 + w}{V_P} \right)^{-1}.$$

This range must be adjusted experimentally. Here is an example of changes in the spectra obtained from the sequences measured by the cutter shown in Fig. 6, *b* when turning 0.1 C-Mn-2 Ni-Mo-V steel at the following cutting conditions: feed rate $S_p = 0.1$ mm, depth of cut $t_p = 1.5$ mm, and cutting speed $V_3 = 1.2$ m/s (Fig. 8).

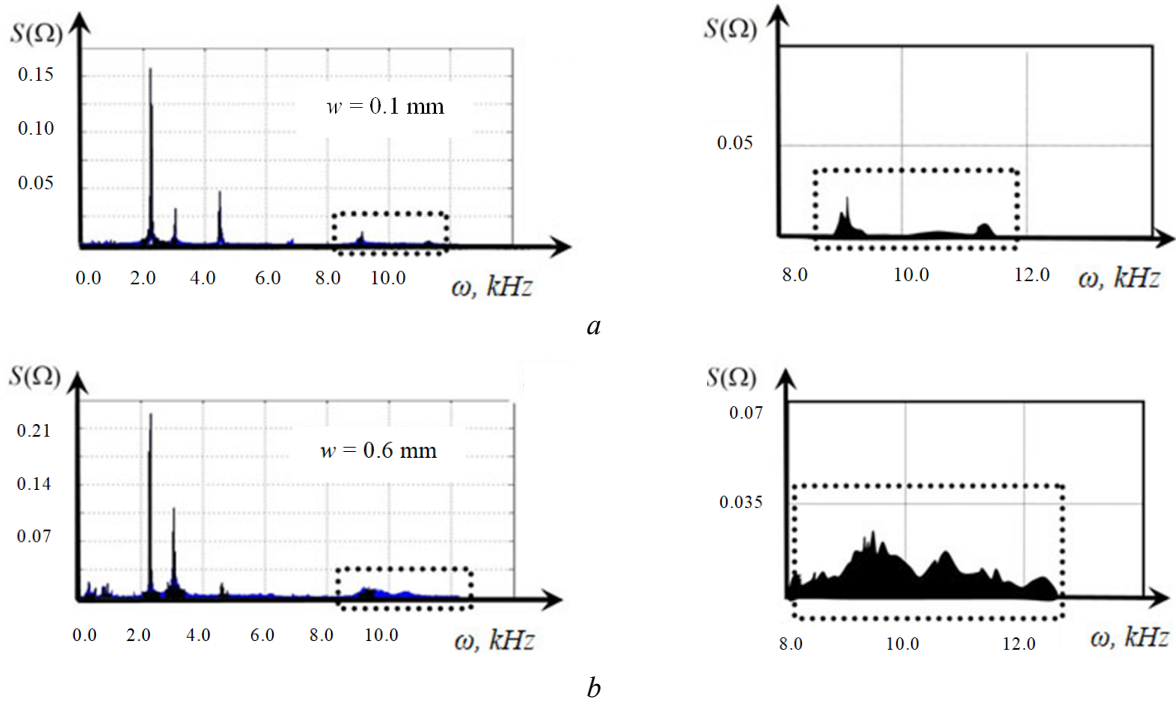


Fig. 8. Example of AE spectrum changes depending on wear

The spectra represent the AE signal measured after the conversion of forces into acoustic waves. Let the vibration sequence $X(t)$ be defined within the frequency window $\Delta\omega_0 \in (\omega_{0,1}, \omega_{0,2})$. Then, the following information features of the AE signal are considered:

$$\Pi_4(w) = \left\{ \int_{\omega_{0,1}}^{\omega_{0,2}} S(\omega, w) d\omega - \int_{\omega_{0,1}}^{\omega_{0,2}} S(\omega, 0) d\omega \right\} \left\{ \int_{\omega_{0,1}}^{\omega_{0,2}} S(\omega, 0) d\omega \right\}^{-1}, \quad (10)$$

where $S(\omega, w)$ is the AE signal spectrum of a worn tool; $S(\omega, 0)$ is the AE signal spectrum at the initial stage of wear.

$$\Pi_5(w) = \left\{ \int_{\omega_{0,1}}^{\omega_{0,c}} S(\omega, w) d\omega - \int_{\omega_{0,c}}^{\omega_{0,2}} S(\omega, 0) d\omega \right\} \left\{ \int_{\omega_{0,1}}^{\omega_{0,2}} S(\omega, 0) d\omega \right\}^{-1}, \quad (11)$$

where $\omega_{0,c}$ is the average frequency of the spectrum within the window $\Delta\omega_0 \in (\omega_{0,1}, \omega_{0,2})$.

Since calculating the frequency within $\Delta\omega_0 \in (\omega_{0,1}, \omega_{0,2})$ can be challenging, it is convenient to select a frequency $\omega_{0,c} = 0.5(\omega_{0,1} + \omega_{0,2})$ and ensure, for $w = 0$, the condition $\int_{\omega_{0,1}}^{\omega_{0,c}} S(\omega, w) d\omega = \int_{\omega_{0,c}}^{\omega_{0,2}} S(\omega, 0) d\omega$ holds.

Finally, to estimate the irregularity of the pulse sequence amplitude, the amplitude modulation signal of the selected high-frequency signal $X(t)$ can be considered. The modulation level of $x(t)$, determined after detecting the signal $X(t)$ and estimating its dispersion using moving average algorithms

$\sigma(t) = \frac{1}{T} \int_{t-\Delta T}^t x(\xi) d\xi$, is highly informative. Then,

$$\Pi_6(w) = \{\sigma_w(t) - \sigma\} \{\sigma\}^{-1}. \quad (12)$$

Depending on the hardware implementation and the vibration sequences available for measurement, all the above-mentioned information features $\Pi = \{\Pi_1, \Pi_2, \dots, \Pi_6\}^T \in \mathbb{R}_{\Pi}^6$ can be used.

All formed information feature set (*IFS*) parameters $\Pi = \{\Pi_1, \Pi_2, \dots, \Pi_6\}^T \in \mathcal{R}_\Pi^6$ have the following properties. First, *IFS* parameters are dimensionless, their values are usually positive, and they change monotonically as wear progresses. Second, wear $w = 0$ in all cases corresponds to the condition $\Pi_i(w) = 0$, when $w = 0$. Third, from the variety of information features, those highly sensitive to changes in wear have been selected. Their area of application depends on the following.

The information feature Π_1 can be used if, as wear progresses, the equilibrium of the dynamic cutting system is asymptotically stable. It suffices to note that the internal amplification factor in the dynamic system depends not only on ρ , but also on the cutting depth. It changes to a lesser extent with variations in cutting speed and feed rate. It has been shown earlier that the evolution of the cutting system properties can be highly sensitive to small variations in technological parameters and disturbances. It can be concluded that the redistribution of amplitudes is highly sensitive to wear development. However, this holds true within the range of stable equilibrium, as well as in cases of low sensitivity of the system evolution to variations in initial system parameters and disturbances.

To use the information feature Π_1 for diagnosing wear on *CNC* machines, it is necessary to coordinate the diagnosis with the *CNC* program. Information assessments Π_2 and Π_3 are more universal but less sensitive to variations in the dynamic properties of the system and to changes in operating modes. When constructing diagnostic systems for turning structural steels at constant cutting modes and stable elastic deformation equilibrium, it is possible to divide wear information into 4–5 wear classes [27].

However, all three characteristics depend on the accuracy of the specific machine and its condition. Previous studies of the coherence function between force disturbances and deformations have shown that it increases with increasing frequency [3]. When selecting the space of information features, the features Π_4 , Π_5 , and Π_6 are more resistant to interference. In this case, the main disturbances are associated with variations in the allowance, spindle group runout, and kinematic disturbances from the feed drives. All disturbances originating from the machine lie within the low-frequency range.

At the same time, when installing the *AE* sensor, it is necessary to take into account the wave properties of the channel connecting the force emission generated in the cutting zone and the measured vibrations (oscillatory deformations, displacements, accelerations, etc.). There is a general rule here: the higher the frequency, the closer the measuring transducer should be to the cutting zone. In our opinion, specialized cutting tools with integrated measurement transducers hold the most promise for *AE* measurement.

The presented method for determining diagnostic signs of tool wear and increased vibration activity of executive elements has practical significance for the creation and development of intelligent algorithms for monitoring systems. Changes in the assessments of diagnostic signs of wear serve as corrective parameters that can be used to build an adaptive control algorithm in the *CNC* unit, capable of extending the tool's service life, but are not limited to this. Within the framework of the presented methodology, the tasks of determining diagnostic signs of degradation of the geometric topology of the part surface and the operational characteristics of the machine tool are of research interest, but these are subjects for future studies. The identified and collected information features in the *VAE* signals allow the creation of "Test Data" and "Training Data" databases for training the assessment of cutting process dynamics in machine learning models of diagnostic systems, which is another step towards the digital transformation of the machine tool industry.

Conclusion

The developed methodology, mathematical modeling, and digital and full-scale experiments have made it possible to form a rational information space for wear diagnosis, in which, based on known recognition methods, decisive rules can be constructed to classify information according to its correspondence to specific wear levels. For the practical application of the methodology in algorithms for monitoring, diagnosing, and controlling the cutting process, it is important to consider the following points.

The basis for constructing tool wear diagnosis systems based on the observation of measurable vibration sequences can be both the dependence of vibrations on changes in the parameters of the dynamic connection

formed by the cutting process and changes in the properties of force emission, represented as a random pulse sequence.

The parameters of the dynamic connection formed by the cutting process depend not only on wear, but also on the technological modes and disturbances originating from the machine itself. Therefore, the use of information parameters based on changes in the vibration spectrum in the low-frequency range is relevant when processing parts in constant modes on equipment with small variations in allowance, spindle group runout, and kinematic disturbances – for example, on automatic production lines. When using these parameters on CNC machines, the diagnostic program must be coordinated with the CNC program; otherwise, the adequacy of wear representation in the spectral characteristics is significantly reduced.

Force emission, considered in the high-frequency range, firstly causes changes in the intensity of force emission; secondly, shifts the intensity maximum within the frequency range; and finally, the development of wear leads to the formation of uncertainty in all parameters modeling force emission as a random pulse process, which is also an informational feature for wear diagnostic systems.

References

1. Budak E. Machining process improvement through process twins. *Proceedings of the 3rd International Conference on the Industry 4.0 Model for Advanced Manufacturing: AMP 2018*. Springer International Publishing, 2018, pp. 164–179. DOI: 10.1007/978-3-319-89563-5_13.
2. Zakovorotny V., Gvindjiliya V. Process control synergetics for metal-cutting machines. *Journal of Vibroengineering*, 2022, vol. 24 (1), pp. 177–189. DOI: 10.21595/jve.2021.22087.
3. Zakovorotnyi V.L., Gvindjiliya V.E. Influence of speeds of forming movements on the properties of geometric topology of the part in longitudinal turning. *Journal of Manufacturing Processes*, 2024, vol. 112, pp. 202–213. DOI: 10.1016/j.jmapro.2024.01.037.
4. Zakovorotny V.L., Gvindjiliya V.E. The study of vibration disturbance mapping in the geometry of the surface formed by turning. *Obrabotka metallov (tekhnologiya, oborudovanie, instrumenty) = Metal Working and Material Science*, 2024, vol. 26, no. 2, pp. 107–126. DOI: 10.17212/1994-6309-2024-26.2-107-126.
5. Ostaf'ev V.A., Antonyuk V.S., Tymchik G.S. *Diagnostika protsessa metalloobrabotki* [Diagnostics of the metalworking process]. Kiev, Tekhnika Publ., 1991. 152 p. ISBN 5-335-00209-3.
6. Kozochkin M.P. Mnogoparametricheskaya diagnostika tekhnologicheskikh sistem dlya obrabotki materialov rezaniem [Multivariate diagnostics of technological systems for processing materials by cutting]. *Vestnik MGTU «Stankin» = Vestnik MSUT «Stankin»*, 2014, no. 1 (28), pp. 13–19.
7. Grubiy S.V. *Optimizatsiya protsessa mekhanicheskoi obrabotki i upravleniya rezhimnymi parametrami* [Optimization of the process of mechanical processing and control of operating parameters]. Moscow, Bauman MSTU Publ., 2014. 149 p. ISBN 978-5-7038-3935-5.
8. Kabaldin Yu.G., Kuzmishina A.M., Shatagin D.A., Anosov M.S. Neironnosetevoe modelirovanie protsessa iznashivaniya tverdosplavnogo instrumenta [Neural network modeling of the wear process of a carbide cutting tool]. *Avtomatizatsiya. Sovremennye tekhnologii = Automation. Modern Technologies*, 2021, vol. 75, no. 9, pp. 398–402. DOI: 10.36652/0869-4931-2021-75-9-398-402.
9. Kabaldin Yu.G., Shatagin D.A., Anosov M.S., Kuzmishina A.M. Razrabotka tsifrovogo dvoynika stanka s ChPU na osnove metodov mashinnogo obucheniya [Development of digital twin of CNC unit based on machine learning methods]. *Vestnik Donskogo gosudarstvennogo tekhnicheskogo universiteta = Vestnik of Don State Technical University*, 2019, no. 19 (1), pp. 45–55. DOI: 10.23947/1992-5980-2019-19-1-45-55.
10. Kabaldin Yu.G., Shatagin D.A., Kuzmishina A.M. Razrabotka tsifrovogo dvoynika rezhushchego instrumenta dlya mekhanoobratyvvayushchego proizvodstva [The development of a digital twin of a cutting tool for mechanical production]. *Izvestiya vysshikh uchebnykh zavedenii. Mashinostroyeniye = Proceedings of Higher Educational Institutions. Machine Building*, 2019, no. 4, pp. 11–17. DOI: 10.18698/0536-1044-2019-4-11-17.
11. Pantyukhin O.V., Vasin S.A. Tsifrovoy dvoynik tekhnologicheskogo protsessa izgotovleniya izdelii spetsial'nogo naznacheniya [Digital double of the technological process of manufacturing special-purpose products]. *Stankoinstrument*, 2021, no. 1 (22), pp. 56–59. DOI: 10.22184/2499-9407.2021.22.1.56.58. (In Russian).



12. Erkorkmaz K., Altintas Y., Yeung C.-H. Virtual computer numerical control system. *CIRP Annals*, 2006, vol. 55 (1), pp. 399–402. DOI: 10.1016/S0007-8506(07)60444-2.
13. Kilic Z.M., Altintas Y. Generalized mechanics and dynamics of metal cutting operations for unified simulations. *International Journal of Machine Tools and Manufacture*, 2016, vol. 104, pp. 1–13. DOI: 10.1016/j.ijmachtools.2016.01.006.
14. Estman L., Merdol D., Brask K.-G., Kalhori V., Altintas Y. Development of machining strategies for aerospace components, using virtual machining tools. *New Production Technologies in Aerospace Industry*. Cham, Springer, 2014, pp. 63–68. DOI: 10.1007/978-3-319-01964-2_9.
15. Kozochkin M.P., Sabirov F.S., Seleznev A.E. Vibroakusticheskii monitoring lezviinoi obrabotki zagotovok iz zakalennoi stali [Vibroacoustic monitoring of cutting edge machining of hardened steel]. *Vestnik MGTU «Stankin» = Vestnik MSUT «Stankin»*, 2018, no. 1 (44), pp. 23–30.
16. Barzov A.A., Gorelov V.A., Igonkin B.A. Akustoelektricheskaya diagnostika protsessa rezaniya polimernykh kompozitsionnykh materialov [Acoustoelectric diagnostics of the cutting process of polymer composite materials]. *Aviatsionnaya promyshlennost' = Aviation Industry*, 1986, no. 12, p. 36.
17. Altintas Y., Kersting P., Biermann D., Budak E., Denkena B. Virtual process systems for part machining operations. *CIRP Annals*, 2014, vol. 63 (2), pp. 585–605. DOI: 10.1016/j.cirp.2014.05.007.
18. Altintas Y., Brecher C., Weck M., Witt S. Virtual machine tool. *CIRP Annals*, 2005, vol. 54 (2), pp. 115–138. DOI: 10.1016/S0007-8506(07)60022-5.
19. Soori M., Arezoo B., Habibi M. Virtual machining considering dimensional, geometrical and tool deflection errors in three-axis CNC milling machines. *Journal of Manufacturing Systems*, 2014, vol. 33 (4), pp. 498–507. DOI: 10.1016/j.jmsy.2014.04.007.
20. Tieng H., Yang H.C., Hung M.H., Cheng F.T. A novel virtual metrology scheme for predicting machining precision of machine tools. *IEEE International Conference on Robotics and Automation*. IEEE, 2013, pp. 264–269. DOI: 10.1109/ICRA.2013.6630586.
21. Astakhov V.P. *Geometry of single-point turning tools and drills: Fundamentals and practical applications*. London, Springer, 2010. 566 p. DOI: 10.1007/978-1-84996-053-3.
22. Konrad H., Isermann R., Oette H.U. Supervision of tool wear and surface quality during end milling operations. *IFAC Proceedings Volumes*, 1994, vol. 27 (4), pp. 507–513. DOI: 10.1016/S1474-6670(17)46074-5.
23. Zakovorotny V.L., Bordachev E.V. Informatsionnoe obespechenie sistemy dinamicheskoi diagnostiki iznosa rezhushchego instrumenta na primere tokarnoi obrabotki [Information support for the system of dynamic diagnostics of cutting tool wear using the example of turning]. *Problemy mashinostroeniya i nadezhnosti mashin = Journal of Machinery Manufacture and Reliability*, 1995, no. 3, pp. 95–103.
24. Grigoriev A.S. Instrumentarii sistemy ChPU dlya diagnostiki i prognozirovaniya iznosa rezhushchego instrumenta v real'nom vremeni pri tokarnoi obrabotke [CNC tool for diagnostic and prediction of cutting tool wear in real time for turning processing]. *Vestnik MGTU «Stankin» = Vestnik MSUT «Stankin»*, 2012, no. 1 (18), pp. 39–43.
25. Zakovorotny V.L., Gvindjiliya V.E. Evolyutsiya dinamicheskoi sistemy rezaniya, obuslovlennaya neobratimymi preobrazovaniyami energii v zone obrabotki [Evolution of the dynamic cutting system caused by irreversible energy transformations in the processing zone]. *STIN = Russian Engineering Research*, 2018, no. 12, pp. 17–25. (In Russian).
26. Zakovorotny V.L., Gvindjiliya V.E. Svyaz' samoorganizatsii dinamicheskoi sistemy rezaniya s iznashivaniem instrumenta [Link between the self-organization of dynamic cutting system and tool wear]. *Izvestiya vuzov. Prikladnaya nelineinaya dinamika = Izvestiya VUZ. Applied Nonlinear Dynamics*, 2020, vol. 28, no. 1, pp. 46–61. DOI: 10.18500/0869-6632-2020-28-1-46-61.
27. Zakovorotny V.L., Gvindjiliya V.E., Kislov K.V. Information properties of frequency characteristics of dynamic cutting systems in the diagnosis of tool wear. *Obrabotka metallov (tekhnologiya, oborudovanie, instrumenty) = Metal Working and Material Science*, 2024, vol. 26, no. 3, pp. 114–134. DOI: 10.17212/1994-6309-2024-26.3-114-134.
28. Rizal M., Ghani J.A., Nuawi M.Z., Haron C.H. A review of sensor system and application in milling process for tool condition monitoring. *Research Journal of Applied Sciences, Engineering and Technology*, 2014, vol. 7 (10), pp. 2083–2097. DOI: 10.19026/rjaset.7.502.
29. Teti R. Advanced IT methods of signal processing and decision making for zero defect manufacturing in machining. *Procedia CIRP*, 2015, vol. 28, pp. 3–15. DOI: 10.1016/j.procir.2015.04.003.



30. Bhuiyan M., Choudhury I., Nukman Y. An innovative approach to monitor the chip formation effect on tool state using acoustic emission in turning. *International Journal of Machine Tools and Manufacture*, 2012, vol. 58, pp. 19–28. DOI: 10.1016/j.ijmachtools.2012.02.001.
31. Rehorn A.G., Jiang J., Orban P.E. State-of-the-art methods and results in tool condition monitoring: a review. *International Journal of Advanced Manufacturing Technology*, 2005, vol. 26, pp. 693–710. DOI: 10.1007/s00170-004-2038-2.
32. Jemielniak K., Arrazola P. Application of AE and cutting force signals in tool condition monitoring in micro-milling. *CIRP Journal of Manufacturing Science and Technology*, 2008, vol. 1 (2), pp. 97–102. DOI: 10.1016/j.cirpj.2008.09.007.
33. Zakovorotny V.L., Ladnik I.V., Dhande S.G. A method for characterization of machine-tools dynamic parameters for diagnostic purposes. *Journal of Materials Processing Technology*, 1995, vol. 53 (3–4), pp. 588–600. DOI: 10.1016/0924-0136(94)01745-M.
34. Zakovorotny V.L., Gvindjiliya V.E. Self-organization and evolution in dynamic friction systems. *Journal of Vibroengineering*, 2021, vol. 23 (6), pp. 1418–1432. DOI: 10.21595/jve.2021.22033.
35. Lee D.E., Hwang I., Valente C.M.O., Oliveira J.F.G., Dornfeld D.A. Precision manufacturing process monitoring with acoustic emission. *International Journal of Machine Tools and Manufacture*, 2006, vol. 46 (2), pp. 176–188. DOI: 10.1016/j.ijmachtools.2005.04.001.
36. Byrne G., Dornfeld D., Inasaki I., Ketteler G., Konig W., Teti R. Tool condition monitoring (TCM) – the status of research and industrial application. *CIRP Annals*, 1995, vol. 44 (2), pp. 541–567. DOI: 10.1016/S0007-8506(07)60503-4.
37. Dimla D.E. Sensor signals for tool-wear monitoring in metal cutting operations – a review of methods. *International Journal of Machine Tools and Manufacture*, 2000, vol. 40 (8), pp. 1073–1098. DOI: 10.1016/S0890-6955(99)00122-4.
38. Choi Y., Narayanaswami R., Chandra A. Tool wear monitoring in ramp cuts in end milling using the wavelet transform. *International Journal of Advanced Manufacturing Technology*, 2004, vol. 23 (5–6), pp. 419–428. DOI: 10.1007/s00170-003-1898-1.
39. Dolinšek S., Kopac J. Acoustic emission signals for tool wear identification. *Wear*, 1999, vol. 225–229 (1), pp. 295–303. DOI: 10.1016/S0043-1648(98)00363-9.
40. Chiou R.Y., Liang S.Y. Analysis of acoustic emission in chatter vibration with tool wear effect in turning. *International Journal of Machine Tools and Manufacture*, 2000, vol. 40 (7), pp. 927–941. DOI: 10.1016/S0890-6955(99)00093-0.
41. Bhuiyan M.S.H., Choudhury I.A., Dahari M., Nukman Y., Dawal S.Z. Application of acoustic emission sensor to investigate the frequency of tool wear and plastic deformation in tool condition monitoring. *Measurement*, 2016, vol. 92, pp. 208–217. DOI: 10.1016/j.measurement.2016.06.006.
42. Siddhpura A., Paurobally R. A review of flank wear prediction methods for tool condition monitoring in a turning process. *International Journal of Advanced Manufacturing Technology*, 2013, vol. 65, pp. 371–393. DOI: 10.1007/s00170-012-4177-1.
43. Karandikar J., McLeay T., Turner S., Schmitz T. Tool wear monitoring using naive Bayes classifiers. *International Journal of Advanced Manufacturing Technology*, 2014, vol. 77, pp. 1613–1626. DOI: 10.1007/s00170-014-6560-6.
44. Kene A.P., Choudhury S.K. Analytical modeling of tool health monitoring system using multiple sensor data fusion approach in hard machining. *Measurement*, 2019, vol. 145, pp. 118–129. DOI: 10.1016/j.measurement.2019.05.062.
45. Mohanraj T., Shankar S., Rajasekar R., Sakthivel N., Pramanik A. Tool condition monitoring techniques in milling process – a review. *Journal of Materials Research and Technology*, 2019, vol. 9 (1), pp. 1032–1042. DOI: 10.1016/j.jmrt.2019.10.031.
46. Kalvoda T., Hwang Y.R. A cutter tool monitoring in machining process using Hilbert–Huang transform. *International Journal of Machine Tool and Manufacture*, 2010, vol. 50 (5), pp. 495–501. DOI: 10.1016/j.ijmachtools.2010.01.006.
47. Zakovorotny V.L., Flek M.B. *Dinamika protsessa rezaniya. Sinergeticheskii podkhod* [The dynamics of the cutting process. Synergistic approach]. Rostov-on-Don, Terra Publ., 2005. 880 p. ISBN 5-98254-055-2.



48. Artobolevskii I.I., Bobrovnitskii Yu.I., Genkin M.D. *Vvedenie v akusticheskuyu dinamiku mashin* [Introduction to the acoustic dynamics of machines]. Moscow, Nauka Publ., 1979. 296 p.

49. Zorev N.N., Granovskii G.I., Larin M.N. *Razvitie nauki o rezanii metallov* [Development of the science of metal cutting]. Moscow, Mashinostroenie Publ., 1967. 416 p.

50. Gvindjiliya V.E., Fominov E.V., Moiseev D.V., Gamaleeva E.I. Influence of dynamic characteristics of the turning process on the workpiece surface roughness. *Obrabotka metallov (tekhnologiya, oborudovanie, instrumenty) = Metal Working and Material Science*, 2024, vol. 26, no. 2, pp. 143–157. DOI: 10.17212/1994-6309-2024-26.2-143-157.

51. Makarov A.D. *Optimizatsiya protsessov rezaniya* [Optimization of cutting processes]. Moscow, Mashinostroenie Publ., 1976. 278 p.

Conflicts of Interest

The authors declare no conflict of interest.

© 2025 The Authors. Published by Novosibirsk State Technical University. This is an open access article under the CC BY license (<http://creativecommons.org/licenses/by/4.0>).

